ACS APPLIED ENERGY MATERIALS

www.acsaem.org Article

Atomic Layer-Deposited ZnO Layer on Hydrated Vanadium Dioxide Cathodes against Vanadium Dissolution for Stable Zinc Ion Batteries

Binbin Shuai,[§] Cheng Zhou,[§] Yuqiang Pi,* and Xu Xu*

Cite This: *ACS Appl. Energy Mater.* 2022, 5, 6139–6145 Read Online

ACCESS | Metrics & More | Article Recommendations | Supporting Information

ABSTRACT: Vanadium oxides are considered one of the most promising cathode materials for aqueous zinc ion batteries. However, vanadium dissolution caused by undesirable side reactions greatly decreases the structure stability and capacity retention. In this work, an atomic layer-deposited ZnO layer is uniformly coated on a hydrated vanadium dioxide nanosheet array cathode, which effectively suppresses the vanadium dissolution and side reactions. The resultant cathode displays improved capacity retentions from 74 to 89% after 100 cycles at 0.5 A g^{-1} and from 29 to 71% after 990 cycles at 5 A g^{-1}. Moreover, the structural evolution after electrochemical cycling of the cathode is thoroughly investigated to reveal the protection mechanism. The atomic layer deposition strategy may also be extended to the protection of other cathodes that suffer from the dissolution issue with wide choices of the protection layer materials.

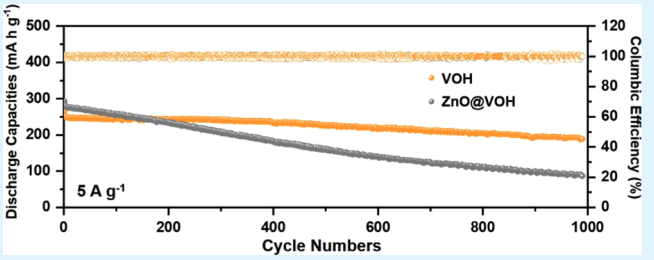

KEYWORDS: *cathode dissolution, artificial solid electrolyte interphase, atomic layer deposition, vanadium oxides, zinc oxide*

1. INTRODUCTION

The development of clean and renewable energy has stimulated a lot of scientific research and development of large-scale energy storage systems with cost-effectiveness and environmental friendliness. In recent years, although more research achievements have been made in lithium-ion batteries using organic electrolytes, some problems caused by organic electrolytes hinder their practical application in energy storage systems, such as the harmful impact on the environment, humidity sensitivity, and potential safety risks caused by a low flash point.[1] Thus, an aqueous battery is considered an attractive candidate for an energy storage system because of its safety and low environmental impact. In particular, aqueous zinc ion batteries (ZIBs) stand out from a variety of water-based batteries and have attracted wide attention of researchers due to the unique advantages of zinc metal anodes, including the low redox potential (−0.76 V *vs* standard hydrogen electrode), chemical stability in water, and rich zinc resources.[2,3] Although zinc metal is undoubtedly the ideal anode for ZIBs, there are still many cathode candidates open for selection.[4] Among them, vanadium oxide cathodes have attracted much attention because of the high reversible capacity and excellent rate capability attributed to the multiple valences of vanadium and the tunable structure of the oxides.[5] However, vanadium dissolution caused by undesirable side reactions greatly decreases the structure stability and capacity retention, limiting their further development and applications.[6]

To solve vanadium dissolution, many strategies have been proposed, such as electrolyte optimization,[7−12] guest species preintercalation,[13−16] surface modification,[17] and so on.[18−21] Electrolyte optimization has been reported as an effective strategy to prevent V dissolution. Zhang et al. designed aqueous organic electrolytes[7,8] and high-concentration electrolytes,[9,10] which can sustain the stable operation of Zn anodes and diverse cathode materials such as vanadium pentoxide, manganese dioxide, and zinc hexacyanoferrate. Various coating materials have been used to improve the stability of the vanadium oxide cathodes in ZIBs. Xu et al. reported poly(3,4-ethylenedioxythiophene) (PEDOT)-coated V_2O_5 nanosheet arrays on carbon cloth as the cathode for ZIBs.[22] The capacity retention of the coated cathode increases from 41 to 89% after 1000 cycles at 5.0 A g^{-1}. Zhang et al. prepared a polypyrrole-coated oxygen-deficient hydrate vanadium dioxide cathode, which exhibited a capacity retention of 85% after 500 cycles at 2 A g^{-1}. The morphology of the coated cathode was retained after cycling, further proving the protective effect of the conducting polymer coating layer.[17] Fan et al. prepared β-VO_2/carbon nanotubes core−shell microspheres as the cathode for ZIBs. The closed core-shell structure with a carbon shell effectively suppresses vanadium dissolution, and

Received: February 18, 2022
Accepted: April 27, 2022
Published: May 9, 2022

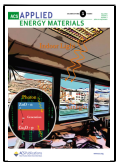

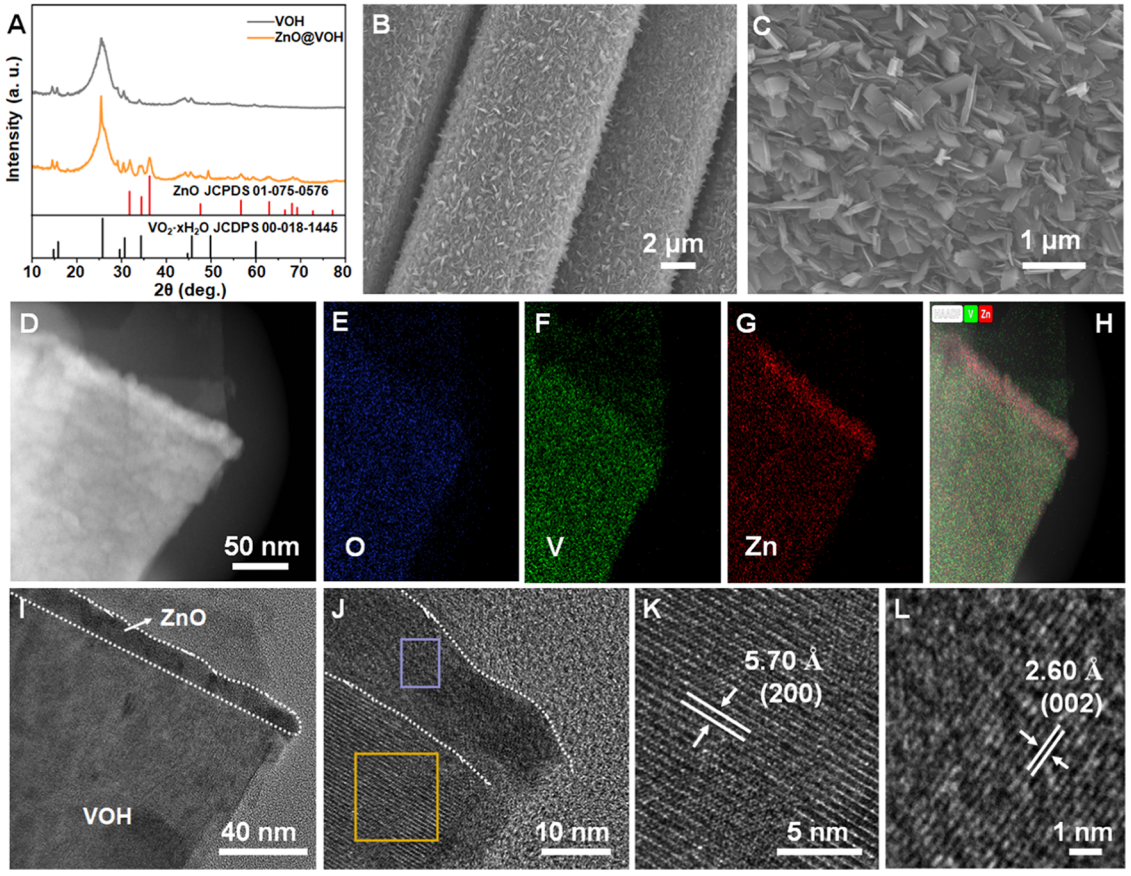

Figure 1. (A) XRD patterns of the VOH and ZnO@VOH; scanning electron microscopy (SEM) images (B, C), high-angle annular dark-field scanning transmission electron microscopy (HAADF-STEM) image (D) with corresponding elemental mapping images (E–H), and TEM images (I–L) of the as-prepared ZnO@VOH.

the cathode maintained a capacity retention of 80% after 7800 cycles.[21]

As one of the most accurate surface-coating methods, atomic layer deposition (ALD) has been widely applied to solve the interfacial issues of the electrodes in various battery systems.[23−26] For the cathode protection in ZIBs, the ultrathin ALD layer with controllable thickness would not only protect the electrode from the undesirable side reaction at the interface to inhibit the cathode dissolution but also act as the artificial cathode electrolyte interphase to allow the transference of zinc ions. Guo et al. first reported an atomic layer-deposited HfO_2 protective layer on the $Zn_3V_2O_7(OH)_2{\cdot}2H_2O$ cathode as an artificial solid electrolyte interphase.[26] The ALD layer with a thickness of only 5 nm effectively suppressed the vanadium dissolution and side reactions without affecting the Zn^{2+} diffusion kinetics. The HfO_2-coated cathode exhibited an improved capacity retention of 84% after 1000 cycles at 10 A g^{-1} compared to 70% of the unmodified cathode.

Herein, an ultrathin ZnO layer is coated on the hydrated vanadium dioxide (VOH) nanosheet array grown on carbon cloth by ALD as the protective layer. The uniform and conformal ZnO layer fully covers the exposed surface of VOH nanosheets and prevents the direct contact between the electrode and the electrolyte, which effectively suppresses the vanadium dissolution and side reactions. The capacity retentions of the coated cathode are improved from 74 to 89% after 100 cycles at 0.5 A g^{-1} and from 29 to 71% after 990 cycles at 5 A g^{-1}.

2. RESULTS AND DISCUSSION

The valuable phase information on the crystalline structure of the as-obtained VOH and ZnO@VOH materials was first characterized by X-ray diffraction (XRD, Figure 1a). All of the diffractions of the VOH can be indexed to the phase of $VO_2{\cdot}xH_2O$ (JCPDS No. 18-1445) without any impurities.[27] The XRD pattern of the ZnO@VOH reveals the presence of ZnO after the ALD process, as the three peaks at 31.9, 34.6, and 36.3° can be ascribed to the characteristic (100), (002), and (101) diffractions of hexagonal ZnO (JCPDS No. 01-075-0576).[28] The strong and sharp diffraction peaks of the ZnO suggest the high crystallinity of the coated ZnO layer.[29] The surface chemical information of VOH and ZnO@VOH materials was further explored by X-ray photoelectron spectroscopy (XPS) measurement. It is obvious that no Zn signal can be detected at the pristine VOH cathode, while the Zn 2p XPS spectra present the strong characteristic peaks at 1044.9 and 1021.7 eV that could match well with the Zn $2p_{1/2}$ and Zn $2p_{3/2}$ signals (Figure S1).[30] The high-resolution XPS spectra of V 2p are given in Figure S2 to further compare the surface chemical state of vanadium in VOH and ZnO@VOH. Both of the spectra can be deconvoluted into the V^{5+} ($2p_{3/2}$: 517.2 eV) and V^{4+} signals ($2p_{3/2}$: 515.9 eV), respectively. The appearance of the V^{5+} signal is a common phenomenon for the VO_2 active material, which could be attributed to the surface oxidation in an air atmosphere.[31] Interestingly, it can be seen that the peak intensity of V^{5+} decreases in the ZnO@VOH (Figure S2), which indicates the relatively lower concentration

https://doi.org/10.1021/acsaem.2c00540
ACS Appl. Energy Mater. 2022, 5, 6139−6145

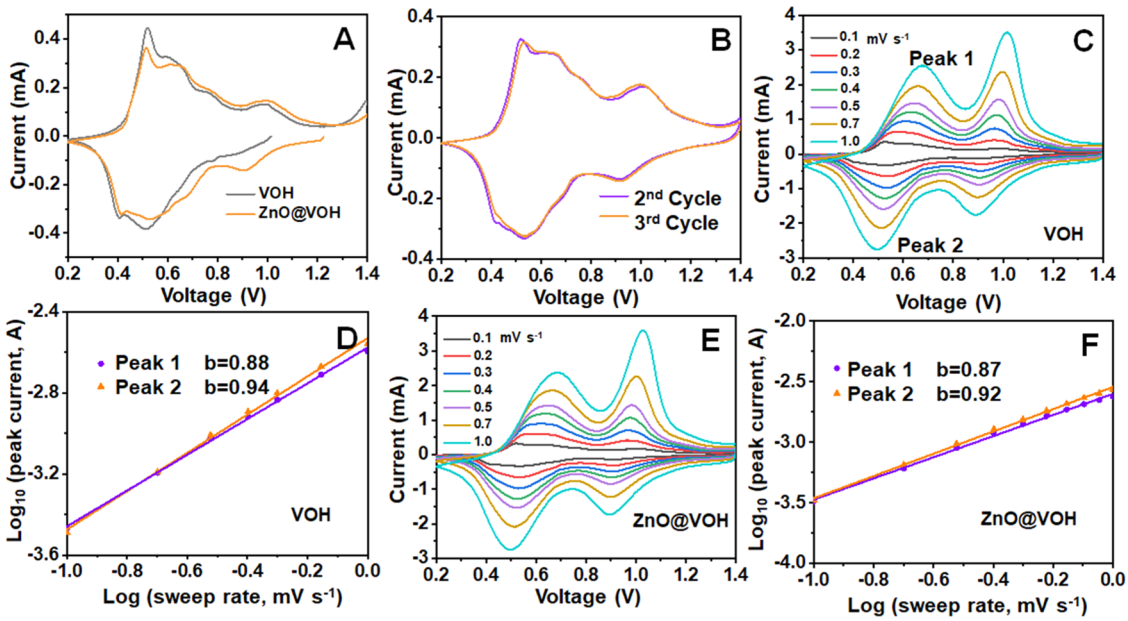

Figure 2. (A) Initial CV curves at 0.1 mV s^{-1} for VOH and ZnO@VOH cathodes; (B) CV curves of ZnO@VOH in the 2nd and 3rd cycles under 0.1 mV s^{-1}; CV curves at 0.1−1.0 mV s^{-1} for VOH (C) and ZnO@VOH (E) cathodes and the corresponding plots of log(i) *vs* log(V) at cathodic/anodic peaks (D, F).

of V^{5+} on the surface. This experimental result demonstrates that the surface ZnO coating could effectively decrease the surface oxidation of the VOH, which could remarkably enhance the chemical stability of the cathode.

The morphologies of the prepared VOH and ZnO@VOH were first examined by scanning electron microscopy (SEM). Both samples present a uniform nanosheet morphology, in which the nanosheets are uniformly and densely loaded on the carbon cloth (Figures 1B, C, S3, and S4). It is evident that the obtained ZnO@VOH can well inherit the overall nanosheet-like morphology of the VOH precursor, as the binding force between VOH and carbon cloth is strong and the coated ZnO layer by ALD technology is conformal and thin. The morphology of the VOH cathode was further investigated by transmission electron microscopy (TEM) characterization. As shown in Figure S5, the VOH exhibits a nanosheet morphology, which is composed of several stacked sheet layers. The lattice fringes with an interplanar spacing of 2.52 Å (Figure S5C) correspond to the (-402) plane of VOH. Then, to better study the microstructure and composition of the ZnO@VOH sample, we explored the HAADF-STEM image and the STEM-energy-dispersive X-ray spectroscopy (EDS) mapping spectrum of the sample (Figure 1D−H). As demonstrated in Figure 1D, a bright rough layer was evenly coated on the surface of the sample, which could be attributed to heavy atoms of Zn.[32] Therefore, it can be speculated that the surface of the VOH sample is successfully coated with a ZnO layer composed of nanoparticles, which is confirmed by the elemental mapping images in Figure 1E−H. Notably, EDS linear scan spectra across the ZnO@VOH nanosheet further show the higher content of Zn on the surface of the nanosheet structure (Figure S6). In Figure 1I,J, clear lattice fringes can be observed on both surface nanoparticles and the interior nanosheet area, suggesting the well-crystallized feature of VOH and ZnO, which is well consistent with the XRD result. The orange and purple regions are further magnified to study the detailed structural information, which is presented in Figure 1K,L. The lattice distance of 5.70 Å corresponds to the (200) plane of $VO_2{\cdot}xH_2O$, while the interplanar spacing of 2.60 Å corresponds to the (002) plane of ZnO. The above XRD, TEM, and XPS characterizations unambiguously demonstrate that the surface of the VOH is successfully coated by the highly crystalline ZnO layer with a thickness of approximately 12 nm, and this ZnO layer is dense as it can effectively prevent the oxidation of surface vanadium under an air atmosphere. Thermogravimetric analysis (TGA) revealed the mass ratio of ZnO in the ZnO@VOH. Based on the results (Figure S7), the mass ratio of ZnO in the total cathode material was 1.2%.

To evaluate the zinc-storage behavior of the VOH and ZnO@VOH cathodes, the electrochemical performances were first evaluated by cyclic voltammetry (CV). The CV curves at a scan rate of 0.1 mV s^{-1} within 0.2−1.4 V in Figure 2A demonstrate the similar electrochemical performance of the VOH and ZnO@VOH cathode, as they show similar peak intensities and peak locations. This experimental phenomenon depicts that the diffusion kinetic of zinc is not hindered by the surface ZnO layer. The multiple pairs of redox peaks in the first cycle indicate the multistep carrier's insertion/desertion process in the active materials. The highly overlapped CV curves of the ZnO@VOH cathode in the 2nd and 3rd cycle (Figure 2B) reveal the highly reversible electrochemical reaction of the electrode, indicating the superior structural stability of the sample. To compare the redox reaction kinetics of VOH and ZnO@VOH cathodes, CV profiles at the scan rates from 0.1 to 1.0 mV s^{-1} were collected in the 0.2−1.4 V range (Figure 2C,E). It is observed that all of the CV curves were able to retain a relatively similar shape with two pairs of distinct redox peaks. However, the peaks in the anodic and cathodic regions tended to shift to the higher and lower voltages resulting from the increased Ohmic losses along with the increased scan rates.[33] However, both exhibited a similar peak position and current under the same scan rate, indicating similar electrochemical kinetics and polarization. Then, the

https://doi.org/10.1021/acsaem.2c00540
ACS Appl. Energy Mater. 2022, 5, 6139−6145

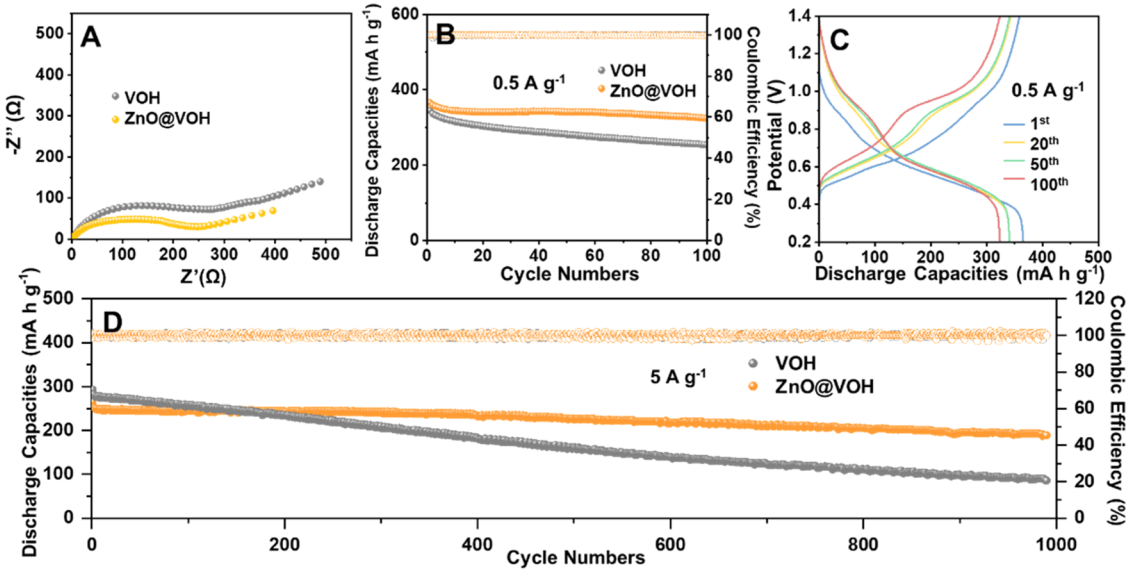

Figure 3. Nyquist plots (A) and cycling performances of the VOH and ZnO@VOH cathodes at 0.5 (B) and 5 A g^{-1} (D); galvanostatic charge/discharge curves for ZnO@VOH at 0.5 A g^{-1} (C).

electrochemical behavior of the batteries was investigated by the calculation of the number of b based on the equation of $I = av^b$ according to the previously reported method.[27,34,35] The value of b close to 0.5 indicates a total diffusion-controlled process caused by the intercalation of carriers, while a b value of 1.0 suggests the surface-controlled capacitive storage process influenced by a surface redox reaction. The b values of VOH (Figure 2D) were determined to be 0.88 (peak 1) and 0.94 (peak 2), while the corresponding b values of ZnO@VOH (Figure 2F) were calculated to be 0.87 (peak 1) and 0.92 (peak 2). This implies that the electrochemical kinetics of VOH and ZnO@VOH electrodes were mainly dominated by the surface-controlled mechanism. The CV curves of ZnO@VOH under 1.0 to 10.0 mV s^{-1} are also shown in Figure S8, and the distinct redox peaks under the high scan rates further confirm the rapid electrochemical reaction kinetics of the sample. Based on this, it is believed that the VOH and ZnO@VOH electrodes present similar electrochemical behavior, and the surface ZnO layer does not hinder the carrier diffusion into the active materials.

Subsequently, electrochemical impedance spectroscopic (EIS) measurements were carried out to further investigate the electrochemical charge transfer kinetics of the VOH and ZnO@VOH cathodes, and Figure 3A shows the Nyquist diagrams of the fresh cells. Obviously, both Nyquist plots were relatively homologous in a semicircle, indicating a similar charge transfer resistance of the samples.[36] To separate the Zn anode contribution, the charge transfer impedance of both materials was tested using a three-electrode system with Ag/AgCl as the reference electrode. The results are shown in Figure S9, and the R_{ct} of the VOH electrode was 0.7 Ω, which increased to 4.2 Ω after the deposition of ZnO. This experimental result confirms that the deposited ZnO layer has little negative effect on the ion transport of the samples. The deposited ZnO is not a fully dense crystalline film, and the presence of boundaries between ZnO crystal grains can also allow Zn^{2+} transport. Moreover, the atomic layer deposition of ZnO creates O and Zn vacancy defects,[37] which are also one of the pathways for Zn^{2+} diffusion. To demonstrate the protective effect of the surface ZnO layer on the electrochemical performance of the samples, a comparison of the cycling performance at current densities of 0.5 and 5 A g^{-1} of the two samples are shown in Figure 3B, D. At a low current density of 0.5 A g^{-1}, the ZnO@VOH exhibits a better cycling performance in comparison with VOH. A high discharge capacity of 365 mA h g^{-1} can be obtained for ZnO@VOH in the first cycle, which is retained as 323 mA h g^{-1} after 100 cycles, corresponding to the capacity retention of 89%. The VOH also delivered a high discharge capacity of 345 mA h g^{-1} in the first cycle; nevertheless, it quickly decreased to 254 mA h g^{-1} after 100 cycles, exhibiting a much lower capacity retention of 74%. After 500 cycles, the capacity retention was 54% for the ZnO@VOH and only 43% for the VOH (Figure S10). Figure 3C shows the corresponding galvanostatic charge-discharge (GCD) curves obtained from the 1st, 20th, 50th, and 100th cycles. The newly emerged plateaus at a potential of 0.90 V correspond to the occurrence of the irreversible phase of $Zn_3V_2O_7(OH)_2{\cdot}2H_2O$, which is consistent with the previous research.[27] The phenomenon could relate to the incomplete reversible insertion/desertion of Zn^{2+}, as the strongly polarizing divalent Zn^{2+} has a strong electrostatic interaction with the host lattice, resulting in the collapse of the original structure during the electrochemical process. Furthermore, the cycling performance of the VOH and ZnO@VOH cathodes under a high current density of 5 A g^{-1} is also compared (Figure 3D). Before the test, the cells were first cycled under 0.5 A g^{-1} for 10 cycles to realize cell activation. The ZnO@VOH showed a satisfactory capacity retention of 71% after 990 cycles, much higher than that of VOH (29%). It is believed that the V-based materials suffer from the dissolution issue in the aqueous electrolyte, leading to quick capacity degradation. With the help of the ALD ZnO layer, the dissolution of vanadium would be partially inhibited and slowed down, resulting in an integrated electrode structure and better cycling performance.

To directly explore the chemical interaction of an aqueous electrolyte with the electrodes, the VOH and ZnO@VOH cathodes were immersed in the electrolyte for 30 days and the electrolyte colors were compared. The electrolyte with VOH changed from colorless to yellow after 30 days, while the electrolyte with ZnO@VOH remained unchanged (Figure

https://doi.org/10.1021/acsaem.2c00540
ACS Appl. Energy Mater. 2022, 5, 6139−6145

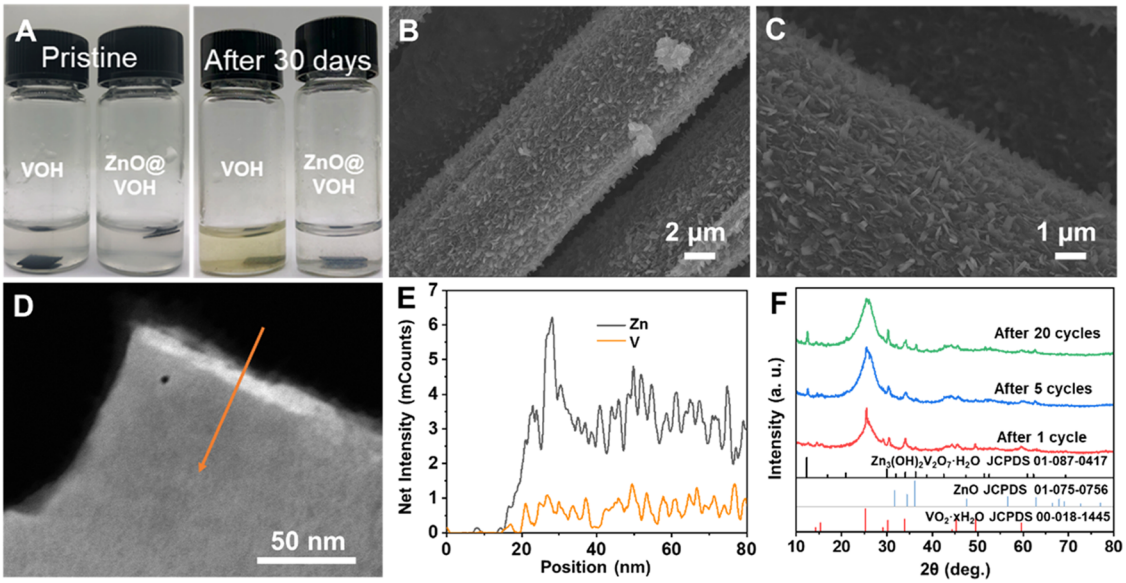

Figure 4. (A) Digital images of the VOH and ZnO@VOH cathodes immersed in the electrolyte;(B, C) SEM images of the ZnO@VOH electrode after 20 cycles; HAADF-STEM image (D) and corresponding linear mappings (E) of the ZnO@VOH electrode; (F) *Ex situ* XRD patterns of the VOH/CC cathode after different cycles.

4A). This evidence clearly confirms that the ALD-coated ZnO could effectively protect VOH from dissolution in the electrolyte. The morphological evolutions of the VOH and ZnO@VOH electrodes cycled at 0.2 A g^{-1} for 20 cycles were also compared by *ex situ* SEM (Figures 4B, C, S11, and S12). The nanosheet morphology of ZnO@VOH was well preserved after the electrochemical process, while the morphology of VOH experienced great change as the nanosheets became irregular and the boundaries between nanosheets became unclear, indicating significant destruction of the nanosheet structure. The *ex situ* HAADF-STEM image of cycled ZnO@VOH also revealed that the surface ZnO layer is well retained as the edge of the nanosheet is much brighter than the rest of the regions (Figure 4D). The EDS linear scan spectra across the cycled ZnO@VOH nanosheet further confirm the higher Zn content on the nanosheet surface (Figure 4E). The strong Zn signal across the nanosheet after cycling may result from the incomplete reversible insertion/desertion of strongly polarizing divalent Zn^{2+} during the electrochemical process. Finally, *ex situ* XRD was applied to investigate the structural evolution after the electrochemical process (Figure 4F). The characteristic diffraction peaks of ZnO disappeared after the tests, corresponding to the amorphization of ZnO after the repeat Zn^{2+} insertion/desertion process. In addition, a new peak at 12.6° appeared after five cycles, and the peak intensity also gradually increased with the cycle numbers. It can be ascribed to the generation of $Zn_3V_2O_7(OH)_2{\cdot}2H_2O$ (JCPDS No. 01-087-0417) in the electrochemical process, which is consistent with the *ex situ* HAADF-STEM image and GCD results. However, the main diffraction peaks of VOH were well retained, which means that the ZnO@VOH is stable during the cycling process. It was found that the surface ZnO layer could not only protect the active materials from dissolution in the electrolyte but also act as a water shield to reduce the insertion of water molecules into the electrode material, finally preventing the irreversible structural transformation during the test and leading to superior cycling stability.

3. CONCLUSIONS

In conclusion, an ultrathin layer of ZnO was fabricated on the surface of a hydrated vanadium dioxide nanosheet array by atomic layer deposition. The crystalline layer was uniformly coated on the nanosheets without changing the morphology, which not only protected the cathode from vanadium dissolution and other side reactions induced by water but also allowed the transport of zinc ions with well-maintained electrochemical kinetics. Benefiting from the protective effect of the ZnO layer, the capacity retentions of the coated cathode improved from 74 to 89% after 100 cycles at 0.5 A g^{-1} and from 29 to 71% after 990 cycles at 5 A g^{-1}. The structural and morphological evolutions of the cathode after cycling were also investigated, which revealed the stability of the ZnO layer and confirmed the protective effect of the ALD layer. This effective strategy may also be extended to the protection of other cathodes suffering from the dissolution issue.

EXPERIMENTAL METHODS

Synthesis of VOH and ZnO@VOH. VOH was synthesized by the hydrothermal method as follows: 2 mmol of V_2O_5 and 6 mmol of $H_2C_2O_4{\cdot}2H_2O$ were dissolved in 12 mL of ultrapure water and stirred at 75 °C for 2 h until a blue-black transparent solution was obtained. When the current bulk solution was cooled down to room temperature, 3 mL of H_2O_2 (30 wt%) solution was added dropwise and stirred for 20 min, and then 65 mL of anhydrous ethanol was added. Then, the pretreated carbon cloth together with the precursor solution was transferred to a poly(tetrafluoroethylene) autoclave. Finally, the hydrothermal reaction was carried out at 180 °C for 100 min. After cooling down to room temperature, the prepared material was removed and washed with ultrapure water and dried to finally obtain VOH. For the preparation of ZnO@VOH, diethyl zinc was used as the zinc source for ALD, and the reaction temperature was 100 °C. ZnO@VOH was obtained after 100 cycles of deposition on VOH. For the preparation of ZnO@VOH, diethyl zinc was used as the zinc source in the atomic layer deposition system (Cambridge Nanotech Savannah S100), and the reaction temperature was 100 °C. Each cycle was as follows: a pulse of water vapor (0.02 s), waiting (20 s), a pulse of diethyl zinc vapor (0.02 s), and waiting again (20 s). ZnO@VOH was obtained after 100 cycles of deposition on VOH.

https://doi.org/10.1021/acsaem.2c00540
ACS Appl. Energy Mater. 2022, 5, 6139−6145

Material Characterization. SEM images were collected using a JEOL JSM-7100F, which can also provide EDS signals. XRD measurements were carried out to perform the crystallographic structural analysis of electrodes on a D8 ADVANCE X-ray diffractometer. TEM was performed using a Titan G2 60-300. XPS spectra were acquired using a VG MultiLab 2000 instrument.

Electrochemical Measurement. The electrodes were cut into small pieces of 1 cm × 1 cm and used as cathodes. The amount of active material loaded on each small piece was about 2 mg cm^{-2}. Using a zinc foil with a diameter of 1.6 cm as the anode, a glass fiber filter membrane as the separator, and 3 M Zn $(CF_3SO_3)_2$ as the electrolyte, the battery was assembled in the shell of a CR2016 coin battery. All of the test coin batteries used in this work were assembled in an indoor room temperature environment. EIS was performed by an electrochemical method with a frequency range of 100 kHz to 0.01 Hz. The constant current charge and discharge test was carried out on the multichannel battery test system (Neware-BTSDA).

■ ASSOCIATED CONTENT

Supporting Information

The Supporting Information is available free of charge at https://pubs.acs.org/doi/10.1021/acsaem.2c00540.

XPS spectra of VOH and ZnO@VOH cathodes; SEM images of the VOH and ZnO@VOH cathodes; TEM images of VOH; EDS linear scan spectrum of ZnO@VOH; CV curves of ZnO@VOH; and SEM images of ZnO@VOH and VOH electrodes after cycling (PDF)

■ AUTHOR INFORMATION

Corresponding Authors

Yuqiang Pi − *School of Chemistry and Materials Science, Hubei Engineering University, Xiaogan 432000, P. R. China*; Email: xq0502@163.com

Xu Xu − *State Key Laboratory of Advanced Technology for Materials Synthesis and Processing, International School of Materials Science and Engineering, Wuhan University of Technology, Wuhan 430070, P. R. China*; orcid.org/0000-0002-3309-7596; Email: xuxu@whut.edu.cn

Authors

Binbin Shuai − *State Key Laboratory of Advanced Technology for Materials Synthesis and Processing, International School of Materials Science and Engineering, Wuhan University of Technology, Wuhan 430070, P. R. China*

Cheng Zhou − *State Key Laboratory of Advanced Technology for Materials Synthesis and Processing, International School of Materials Science and Engineering, Wuhan University of Technology, Wuhan 430070, P. R. China*

Complete contact information is available at: https://pubs.acs.org/10.1021/acsaem.2c00540

Author Contributions

§B.S. and C.Z. contributed equally to this work. The manuscript was written through contributions of all authors. All authors have given approval to the final version of the manuscript.

Notes

The authors declare no competing financial interest.

■ ACKNOWLEDGMENTS

This work was supported by the National Natural Science Foundation of China (51702247), the Fundamental Research Funds for the Central Universities (WUT: 2021IVA123, 2021III009JC, 2021III013GL), the Hainan Provincial Joint Project of Sanya Yazhou Bay Science and Technology City (520LH056), and Sanya Science and Education Innovation Park of Wuhan University of Technology (2020KF0021). The authors thank Prof. Ping Wei of the Nanostructure Research Center (NRC) at Wuhan University of Technology for the TEM test.

■ REFERENCES

(1) Liu, Z.; Huang, Y.; Huang, Y.; Yang, Q.; Li, X.; Huang, Z.; Zhi, C. Voltage issue of aqueous rechargeable metal-ion batteries. *Chem. Soc. Rev.* **2020**, *49*, 180−232.

(2) Zhang, N.; Chen, X.; Yu, M.; Niu, Z.; Cheng, F.; Chen, J. Materials chemistry for rechargeable zinc-ion batteries. *Chem. Soc. Rev.* **2020**, *49*, 4203−4219.

(3) Hao, J.; Li, X.; Zeng, X.; Li, D.; Mao, J.; Guo, Z. Deeply understanding the Zn anode behaviour and corresponding improvement strategies in different aqueous Zn-based batteries. *Energy Environ. Sci.* **2020**, *13*, 3917−3949.

(4) Yong, B.; Ma, D.; Wang, Y.; Mi, H.; He, C.; Zhang, P. Understanding the Design Principles of Advanced Aqueous Zinc-Ion Battery Cathodes: From Transport Kinetics to Structural Engineering, and Future Perspectives. *Adv. Energy Mater.* **2020**, *10*, No. 2002354.

(5) Kundu, D.; Adams, B. D.; Duffort, V.; Vajargah, S. H.; Nazar, L. F. A high-capacity and long-life aqueous rechargeable zinc battery using a metal oxide intercalation cathode. *Nat. Energy* **2016**, *1*, No. 16119.

(6) Lin, C.; Qi, F.; Dong, H.; Li, X.; Shen, C.; Ang, E. H.; Han, Y.; Geng, H.; Li, C. C. Suppressing vanadium dissolution of V_2O_5via in situ polyethylene glycol intercalation towards ultralong lifetime room/low-temperature zinc-ion batteries. *Nanoscale* **2021**, *13*, 17040−17048.

(7) Dong, Y.; Miao, L.; Ma, G.; Di, S.; Wang, Y.; Wang, L.; Xu, J.; Zhang, N. Non-concentrated aqueous electrolytes with organic solvent additives for stable zinc batteries. *Chem. Sci.* **2021**, *12*, 5843−5852.

(8) Ma, G.; Miao, L.; Dong, Y.; Yuan, W.; Nie, X.; Di, S.; Wang, Y.; Wang, L.; Zhang, N. Reshaping the electrolyte structure and interface chemistry for stable aqueous zinc batteries. *Energy Storage Mater.* **2022**, *47*, 203−210.

(9) Zhang, N.; Dong, Y.; Jia, M.; Bian, X.; Wang, Y.; Qiu, M.; Xu, J.; Liu, Y.; Jiao, L.; Cheng, F. Rechargeable aqueous Zn−V_2O_5 battery with high energy density and long cycle life. *ACS Energy Lett.* **2018**, *3*, 1366−1372.

(10) Li, C.; Yuan, W.; Li, C.; Wang, H.; Wang, L.; Liu, Y.; Zhang, N. Boosting $Li_3V_2(PO_4)_3$ cathode stability using a concentrated aqueous electrolyte for high-voltage zinc batteries. *Chem. Commun.* **2021**, *57*, 4319−4322.

(11) Zhang, L.; Zhang, B.; Hu, J.; Liu, J.; Miao, L.; Jiang, J. An In Situ Artificial Cathode Electrolyte Interphase Strategy for Suppressing Cathode Dissolution in Aqueous Zinc Ion Batteries. *Small Methods* **2021**, *5*, No. 2100094.

(12) Zhang, D.; Cao, J.; Yue, Y.; Pakornchote, T.; Bovornratanaraks, T.; Han, J.; Zhang, X.; Qin, J.; Huang, Y. Two Birds with One Stone: Boosting Zinc-Ion Insertion/Extraction Kinetics and Suppressing Vanadium Dissolution of V_2O_5 via La^{3+} Incorporation Enable Advanced Zinc-Ion Batteries. *ACS Appl. Mater. Interfaces* **2021**, *13*, 38416−38424.

(13) Li, R.; Xing, F.; Li, T.; Zhang, H.; Yan, J.; Zheng, Q.; Li, X. Intercalated polyaniline in V_2O_5 as a unique vanadium oxide bronze cathode for highly stable aqueous zinc ion battery. *Energy Storage Mater.* **2021**, *38*, 590−598.

(14) Liu, Y.; Zou, Y.; Guo, M.; Hui, Z.; Zhao, L. Boosting the active sites and kinetics of VO_2 by Mn pre-intercalated and PVP modified nanostructure to improve the cycle stability for aqueous zinc batteries. *Chem. Eng. J.* **2022**, *433*, No. 133528.

(15) Li, W.; Han, C.; Gu, Q.; Chou, S. L.; Wang, J. Z.; Liu, H. K.; Dou, S. X. Electron Delocalization and Dissolution-Restraint in Vanadium Oxide Superlattices to Boost Electrochemical Performance

of Aqueous Zinc-Ion Batteries. *Adv. Energy Mater.* **2020**, *10*, No. 2001852.
(16) Yin, C.; Pan, C.; Liao, X.; Pan, Y.; Yuan, L. Regulating the Interlayer Spacing of Vanadium Oxide by In Situ Polyaniline Intercalation Enables an Improved Aqueous Zinc-Ion Storage Performance. *ACS Appl. Mater. Interfaces* **2021**, *13*, 39347−39354.
(17) Zhang, Z.; Xi, B.; Wang, X.; Ma, X.; Chen, W.; Feng, J.; Xiong, S. Oxygen Defects Engineering of VO_2 xH_2O Nanosheets via In Situ Polypyrrole Polymerization for Efficient Aqueous Zinc Ion Storage. *Adv. Funct. Mater.* **2021**, *31*, No. 2103070.
(18) Wang, X.; Xi, B.; Ma, X.; Feng, Z.; Jia, Y.; Feng, J.; Qian, Y.; Xiong, S. Boosting Zinc-Ion Storage Capability by Effectively Suppressing Vanadium Dissolution Based on Robust Layered Barium Vanadate. *Nano Lett.* **2020**, *20*, 2899−2906.
(19) Zhang, L.; Hu, J.; Zhang, B.; Liu, J.; Wan, H.; Miao, L.; Jiang, J. Suppressing cathode dissolution via guest engineering for durable aqueous zinc-ion batteries. *J. Mater. Chem. A* **2021**, *9*, 7631−7639.
(20) Liu, T.; Xu, Z.; Chen, L.; Zhang, Y.; Wang, M.; Jia, Y.; Huang, Y. Boosting zinc ion storage performance of sandwich-like V_2O_5/graphene composite by effectively inhibiting vanadium dissolution. *J. Colloid Interface Sci.* **2022**, *613*, 524−535.
(21) Fan, X.; Wen, X.; Tang, Y.; Zhou, W.; Xiang, K.; Chen, H. β-VO_2/carbon nanotubes core-shelled microspheres and their applications for advanced cathode in aqueous zinc ion batteries. *Electrochim. Acta* **2021**, *400*, No. 139425.
(22) Xu, D.; Wang, H.; Li, F.; Guan, Z.; Wang, R.; He, B.; Gong, Y.; Hu, X. Conformal Conducting Polymer Shells on V_2O_5 Nanosheet Arrays as a High-Rate and Stable Zinc-Ion Battery Cathode. *Adv. Mater. Interfaces* **2019**, *6*, No. 1801506.
(23) Zeng, Z.; Zeng, Y.; Sun, L.; Mi, H.; Deng, L.; Zhang, P.; Ren, X.; Li, Y. Long cyclic stability of acidic aqueous zinc-ion batteries achieved by atomic layer deposition: the effect of the induced orientation growth of the Zn anode. *Nanoscale* **2021**, *13*, 12223−12232.
(24) Liu, X.; Li, Z.; Liao, X.; Hong, X.; Li, Y.; Zhou, C.; Zhao, Y.; Xu, X.; Mai, L. A three-dimensional nitrogen-doped graphene framework decorated with an atomic layer deposited ultrathin V2O5 layer for lithium sulfur batteries with high sulfur loading. *J. Mater. Chem. A* **2020**, *8*, 12106−12113.
(25) Zhao, K.; Wang, C.; Yu, Y.; Yan, M.; Wei, Q.; He, P.; Dong, Y.; Zhang, Z.; Wang, X.; Mai, L. Ultrathin Surface Coating Enables Stabilized Zinc Metal Anode. *Adv. Mater. Interfaces* **2018**, *5*, No. 1800848.
(26) Guo, J.; Ming, J.; Lei, Y.; Zhang, W.; Xia, C.; Cui, Y.; Alshareef, H. N. Artificial Solid Electrolyte Interphase for Suppressing Surface Reactions and Cathode Dissolution in Aqueous Zinc Ion Batteries. *ACS Energy Lett.* **2019**, *4*, 2776−2781.
(27) Tao, Y.; Huang, D.; Chen, H.; Luo, Y. Electrochemical Generation of Hydrated Zinc Vanadium Oxide with Boosted Intercalation Pseudocapacitive Storage for a High-Rate Flexible Zinc-Ion Battery. *ACS Appl. Mater. Interfaces* **2021**, *13*, 16576−16584.
(28) Hossain, M. M.; Shima, H.; Islam, M. A.; Hasan, M.; Lee, M. Simple synthesis process for ZnO sphere-decorated CNT fiber and its electrical, optical, thermal, and mechanical properties. *RSC Adv.* **2016**, *6*, 4683−4694.
(29) Yang, B.; Li, L.; Jia, Z.; Liu, X.; Zhang, C.; Guo, L. Comparative study of CO_2 hydrogenation to methanol on cubic bixbyite-type and rhombohedral corundum-type indium oxide. *Chin. Chem. Lett.* **2020**, *31*, 2627−2633.
(30) Akcay, N.; Gremenok, V.; Ivanov, V. A.; Zaretskaya, E.; Ozcelik, S. Characterization of Cu_2ZnSnS_4 thin films prepared with and without thin Al_2O_3 barrier layer. *Sol. Energy* **2022**, *234*, 137−151.
(31) Cui, F.; Zhao, J.; Zhang, D.; Fang, Y.; Hu, F.; Zhu, K. VO_2(B) nanobelts and reduced graphene oxides composites as cathode materials for low-cost rechargeable aqueous zinc ion batteries. *Chem. Eng. J.* **2020**, *390*, No. 124118.
(32) Liu, Z.; Sun, F.; Gu, L.; Chen, G.; Shang, T. T.; Liu, J.; Le, Z. Y.; Li, X. Y.; Wu, H. B.; Lu, Y. F. Post Iron Decoration of Mesoporous Nitrogen-Doped Carbon Spheres for Efficient Electrochemical Oxygen Reduction. *Adv. Energy Mater.* **2017**, *7*, No. 1701154.
(33) Cui, F. H.; Wang, D. S.; Hu, F.; Yu, X.; Guan, C.; Song, G. H.; Xu, F.; Zhu, K. Deficiency and surface engineering boosting electronic and ionic kinetics in NH4V4O10 for high-performance aqueous zinc-ion battery. *Energy Storage Mater.* **2022**, *44*, 197−205.
(34) Zhu, X. D.; Cao, Z. Y.; Wang, W. J.; Li, H. J.; Dong, J. C.; Gao, S. P.; Xu, D. X.; Li, L.; Shen, J. F.; Ye, M. X. Superior-Performance Aqueous Zinc-Ion Batteries Based on the In Situ Growth of MnO2 Nanosheets on V_2CTX MXene. *ACS Nano* **2021**, *15*, 2971−2983.
(35) He, P.; Quan, Y.; Xu, X.; Yan, M.; Yang, W.; An, Q.; He, L.; Mai, L. High-Performance Aqueous Zinc-Ion Battery Based on Layered $H_2V_3O_8$ Nanowire Cathode. *Small* **2017**, *13*, No. 1702251.
(36) Wei, J. F.; Li, B. C.; Jing, L. Y.; Tian, N.; Zhao, X.; Zhang, J. P. Efficient protection of Mg alloy enabled by combination of a conventional anti-corrosion coating and a superamphiphobic coating. *Chem. Eng. J.* **2020**, *390*, No. 124562.
(37) Kayaci, F.; Vempati, S.; Donmez, I.; Biyikli, N.; Uyar, T. Role of zinc interstitials and oxygen vacancies of ZnO in photocatalysis: a bottom-up approach to control defect density. *Nanoscale* **2014**, *6*, 10224−10234.

https://doi.org/10.1021/acsaem.2c00540
ACS Appl. Energy Mater. 2022, 5, 6139−6145